



# A Novel Method to Measure Equi-Biaxial Residual Stress by Nanoindentation

A. Greco<sup>1</sup> · E. Sgambitterra<sup>1</sup> · F. Furgiuele<sup>1</sup> · D. Furfari<sup>2</sup>

Received: 1 June 2023 / Accepted: 31 August 2023 / Published online: 10 October 2023  
© The Author(s) 2023

## Abstract

**Background** The accurate measurement of residual stresses (RS) is crucial for predicting the performance of mechanical components, as RS can significantly impact fatigue life, fracture, corrosion, and wear resistance. Different experimental methods were developed to measure RS, including non-destructive techniques. Among these methods, instrumented nanoindentation has emerged as a promising approach to assess equi- or non-equi-biaxial RS states. This technique analyzes variations in the mechanical response of indentation on a stressed or stress-free component to estimate residual stresses. Previous studies proposed different approaches to establish a relationship between RS and indentation parameters, such as contact area, peak load, mean contact pressure, indentation work, etc. However, the correlation between RS and peak load variation, commonly assumed to be linear, showed limitations, particularly when dealing with compressive RS.

**Objective** The aim of this work is to develop a hybrid procedure, based on finite element (FEM) simulations and experimental analyses, to measure the equi-biaxial residual stresses. In particular, it is based on the analysis of the nanoindentation peak load variation generated by the presence of residual stresses on a component.

**Methods** To overcome the limitations of the linear assumption, nanoindentation experiments were combined with finite element analyses (FEA). FEA simulations were used to estimate the correlation between RS and peak load variation, providing a better understanding of the non-linear relationship. A proper experimental setup, consisting in a stress generating jig, was designed and manufactured to perform nanoindentations on a sample, made by aluminium alloy AA 7050 T451, subjected to external mechanical stress with the aim to validate the FEA model. FEA and the digital image correlation (DIC) technique were also used to verify that the induced stress field was the expected one.

**Results** Obtained results revealed that the proposed method is a valid way to measure residual stresses. In fact, it offers an improved correlation between RS and peak load variation. In addition, by integrating nanoindentation experiments and FEA, a more accurate assessment of RS can be also achieved.

**Conclusions** This research contributes to the development of a consistent methodology for RS measurement using instrumented nanoindentation.

**Keywords** Residual Stress Measurement · Nano-indentation · Digital Image Correlation · Finite Element Simulation

## Introduction

The performances of mechanical components are strongly affected by the presence of residual stresses (RS). According to their sign and combined with the applied stress field, they

can be beneficial or detrimental for the fatigue life, fracture, oxygen crack corrosion and wear resistance. The prediction of components performance highly depends on the correct measurement of RS field [1–5]. Mostly in general, the RS field can be classified as equi- or non-equi-biaxial, according to the sign and the magnitude of the principal RS components. In particular, when their sign and magnitude are the same, the RS stress state is named equi-biaxial, otherwise, non-equi-biaxial.

Over the years, several experimental methods were developed to measure residual stresses [6, 7] and, typically, they are classified as non-destructive, semi-destructive

✉ E. Sgambitterra  
emanuele.sgambitterra@unical.it

<sup>1</sup> Department of Mechanical, Energy and Management Engineering, University of Calabria, Rende, CS, Italy

<sup>2</sup> Airbus Operations GmbH, ZAL Tech Center, Hein-Saß-Weg 22, Hamburg 21129, Germany

or destructive. Among the non-destructive methods, the instrumented nanoindentation is one of the youngest and, therefore, more efforts are required to make it as a consistent and certified methodology. Nanoindentation, in particular, allows to obtain an accurate measure of the equi- or non-equi-biaxial RS state on the surface of components at the nanoscale [8]. The basic idea in measuring equi-biaxial RS field using nanoindentation is to analyse the variations in the mechanical indentation response on a component under stress-free conditions or under the effect of RS [8–10]. In fact, it was widely demonstrated that the presence of RS modifies the peak load, the contact area or the mean contact pressure compared to a stress-free case. Starting from this remark, different approaches were developed over the years [9, 11–15] to establish a relation between RS and indentation parameters.

In particular, Suresh et al. [11] exploited the contact area variation to determine RS; Lee et al. [12] assumed a linear relation between RS and the peak load variation. This latter, in particular, represents the difference of the load, measured at the maximum penetration depth, between a sample in stress free conditions and a sample under the effect of residual stresses. The methodology proposed by Swadener et al. [13] is based on the relation between the mean contact pressure variation generated by the presence of RS; Xu et al. [14, 15] found the dependence of the elastic recovery to the maximum penetration depth ratio on RS. Lu et al. [16] used the loading curvature variation for the RS determination; Wang et al. [17] adopted an energy method to determine the difference in the indentation work between stressed and stress-free sample; Pham et al. [18] used a sharp indentation load-depth curve to measure simultaneously RS and plastic properties in steels. For the sake of clarity, Table 1 summarizes some of the methodologies proposed in literature; the precision of the previous methods depends on the specific case [19–21].

Recent progress involves the use of finite element analyses (FEA), coupled with indentation tests, for the RS

measurement RS [22–25]. Hosseinzadeh et al. [22] determine RS and material properties combining the load-depth curve with FEA and genetic algorithms. Finite element simulations and sharp indentation tests were also used by Wang et al. [23] for determining the welding-induced RS. Moharrami et al. [24] uses FEA to improve the accuracy of the Lee's method [12] by determining and correcting the error committed by the Lee's prediction for different set of RS ratio and yield strain. Peng et al. [25] proposed a method based on the indentation energy difference between stressed and stress-free samples in the indentation loading path; in particular, FEAs were used to determine the dependence of the elastic and plastic indentation energy on RS. The RS produced by welding were determined also by Lee et al. [26] and by Xue et al. [27] using indentation technique, FEA and optical observation.

The aim of this work is to propose an effective method for the residual stresses measurement that can be applied to a wide range of materials at the nanoscale using a sharp Berkovich indenter. Among the different parameters proposed in literature to measure residual stresses, the peak load was selected as the estimator. This latter, in fact, is the most convenient as it is directly measured, with high accuracy, by the nanoindenter. According to Lee et al. [12], that also used the peak load for RS determination, a linear relation between RS and peak load variation can be assumed. However, several studies demonstrated that this relation is not linear as the compressive RS have a higher effect on the nanoindentation curves than the tensile ones [11, 16, 28, 30, 31], leading in measurement error when Lee's method is used.

The aim of the present paper is to provide a methodology that is simple, accurate, applicable to a wide range of ductile materials and that allow to overcome Lee's model [12] limitations by finding a better correlation between the peak load variation and residual stresses. To this aim both nanoindentation experiments and numerical FEA were exploited. In particular, FEA analyses were used to estimate the correlation between the RS and peak load variation. A

**Table 1** Summary of the most used RS measurement methodologies based on indentation technique

| Article              | Scale      | Parameter of analysis | Indenter type | Main limitation  |
|----------------------|------------|-----------------------|---------------|--|
| Suresh et al. [11]   | Macroscale | Contact area          | Sharp         | Suitable for materials that exhibit sink-in phenomena [9].   |
| Lee et al. [12]      | Macroscale | Peak load             | Sharp         | Assumption of linear relation between RS and peak load [11, 16, 28].                                     |
| Swadener et al. [13] | Nanoscale  | Mean contact pressure | Blunt         | Not suitable to thin films and materials that tends to pile-up [13, 29].                                 |
| Xu et al. [14, 15]   | Nanoscale  | Elastic recovery      | Sharp         | Application limited to very hard materials (low value of the ratio elastic modulus to yield stress) [9]. |
| Lu et al. [16]       | Macroscale | Loading curvature     | Sharp         | Measurement variable indirectly obtained and consistent measurement error (up to 28%) [16].              |
| Wang et al. [17]     | Nanoscale  | Indentation work      | Sharp         | Accurate for materials with high strain hardening exponents and yield strains [20].                      |

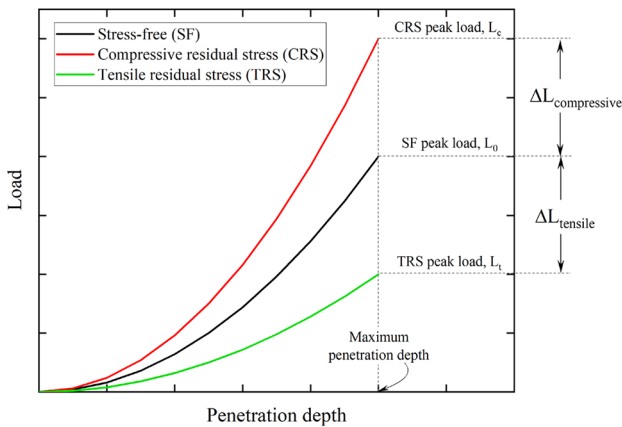


**Fig. 1** Scheme of the residual stress effect on the nanoindentation curves

proper experimental setup was developed to carry out nanoindentation on a sample under the effect of an external mechanical stress. Obtained data, in terms of experimental peak load variation as a function of the applied stress, were used to validate the model. The main advantage of the proposed method is represented by the parameter selected for the analysis, i.e. the peak load, that is directly measured by the nanoindenter, reducing the data processing time and increasing the accuracy of the measurements. Furthermore, the combination of experiments and Finite Element Analysis allows to find a non-linear correlation between RS and peak load with low experimental efforts and increasing the accuracy of the measurements.

It is important to point out that, this method can be applied in several cases if the material properties are well known. These latter can be obtained from a virgin dog-bone

stress-free sample, before starting the RS measurement, using standard tensile test.

### Methodology

The proposed method comes from the effect that RS have on the nanoindentation responses, as schematically shown in Fig. 1. In particular, when nanoindentation tests are carried out in depth control mode, the maximum recorded load is strongly dependent by the presence of residual stresses. Naming  $L_0$  the peak load required to penetrate the stress-free sample until a specific maximum penetration depth, one can observe that it will get modified according to the sign of the residual stress. In detail, when the sample is under the effect of compressive residual stress (CRS) the maximum load  $L_c$  is greater than  $L_0$ , whereas when the sample is under the effect of tensile residual stress (TRS) the maximum load  $L_t$  is smaller than  $L_0$ .

Based on these considerations, a relation between RS and the nanoindentation peak loads can be univocally determined. For a better understanding, a flowchart diagram of the methodology is depicted in Fig. 2. It can be divided into 2 major steps: preliminary numerical analyses and measurement step. Within the preliminary step: i) the maximum penetration depth to be used for the numerical indentations of both the samples, i.e. the one under stress free conditions and the one under the effect of the numerically applied residual stresses, must be specified; ii) the nanoindentation peak load  $L_0$  on the stress free sample is determined; iii) accordingly, the nanoindentation peak load  $L$  on the sample under the effect of the applied residual stresses is numerically determined as

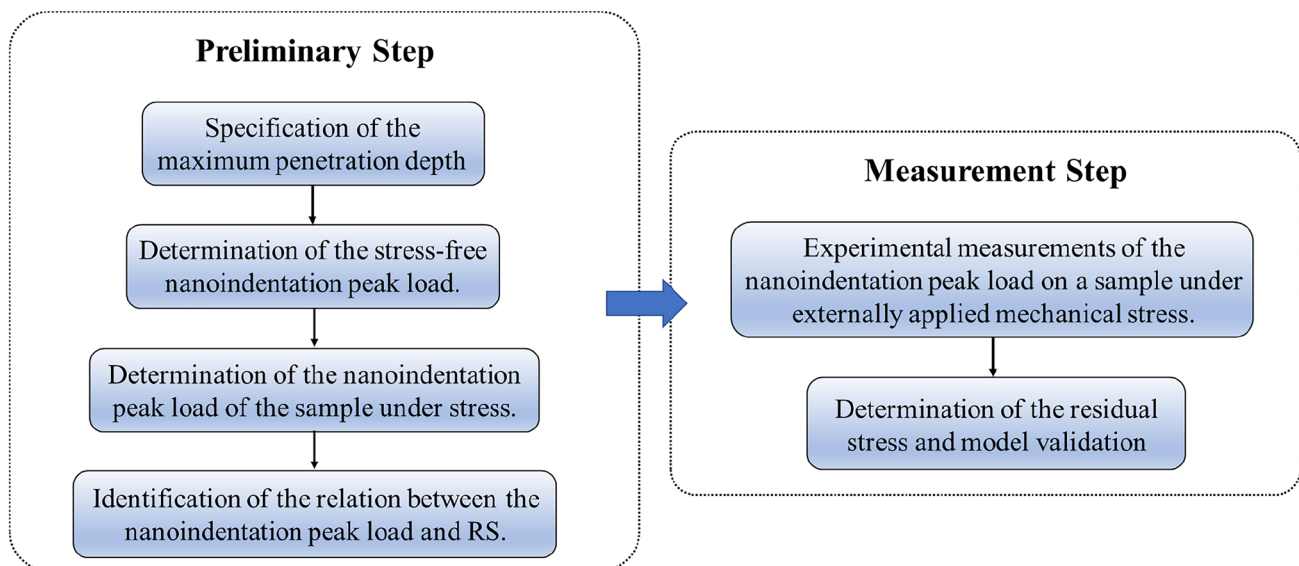


**Fig. 2** Flowchart diagram of the proposed residual stress measurement method

well, finally; iv) a relation between RS and nanoindentation peak load must be established. Within the measurement step: i) the specimen under the effect of externally applied stresses is indented until the previously specified maximum penetration depth and the maximum load  $L$  is recorded; ii) using the correlation between RS and nanoindentation load, estimated in the preliminary step, the estimation of the RS will be validated.

It should be noted that for the estimation of the RS both the nanoindentation peak load  $L$  and the relative nanoindentation load variation  $\delta L$ , calculated according to equation (1), can be used:

$$\delta L = \frac{L - L_0}{L_0} \quad (1)$$

Furthermore, the stress-free nanoindentation load  $L_0$  can be determined or experimentally, if a reference stress-free sample is available, or by finite element analyses. In this latter case, the constitutive behaviour of the material has to be known. The relation between RS and nanoindentation load  $L$ , or relative nanoindentation load variation  $\delta L$  can be determined via FEM.

### FEM Nanoindentation Model

A finite element model was built using the commercial code ABAQUS CAE (Dassault Systemes 2020) to simulate the nanoindentation process and to quantitatively derive

the relation between RS and nanoindentation load  $L$ , as described in "Methodology" section.

The FEM model is made by 2 different parts: the sample and the Berkovich indenter; this latter was modelled as an equivalent cone with an apex angle of  $70.3^\circ$  without generating big simulation errors as demonstrated by Koloor et al. [32], Celentano et al. [33] and Fischer-Cripps [34]. Because of the symmetry conditions, only a quarter of the entire bodies was modelled. The indenter was defined as a discrete rigid part discretized in about 18,000 R3D4 elements. The specimen was modelled as a deformable part discretized in about 150,000 C3D4 elements. Mesh was refined near the contact zone to improve the accuracy of the results. The sizes of the whole model are 2 orders of magnitude greater than the contact zone sizes to avoid effect of the boundary conditions on the simulation. Figure 3 shows the FEM assembly, with a highlight of the contact zone.

The interaction between the bodies was managed through the definition of a master surface (indenter) and a slave surface (specimen). A frictionless contact was defined since it was widely shown that friction effect on the maximum load is totally negligible [8]. Residual stresses were modelled as uniformly distributed pressure over the surfaces with normal along the  $x$  and  $z$  directions (Fig. 3) that are not involved in boundary symmetry conditions. The specimen was made of AA 7050 T451. Both elastic and plastic properties of the specimen material were implemented in the model. All the mechanical

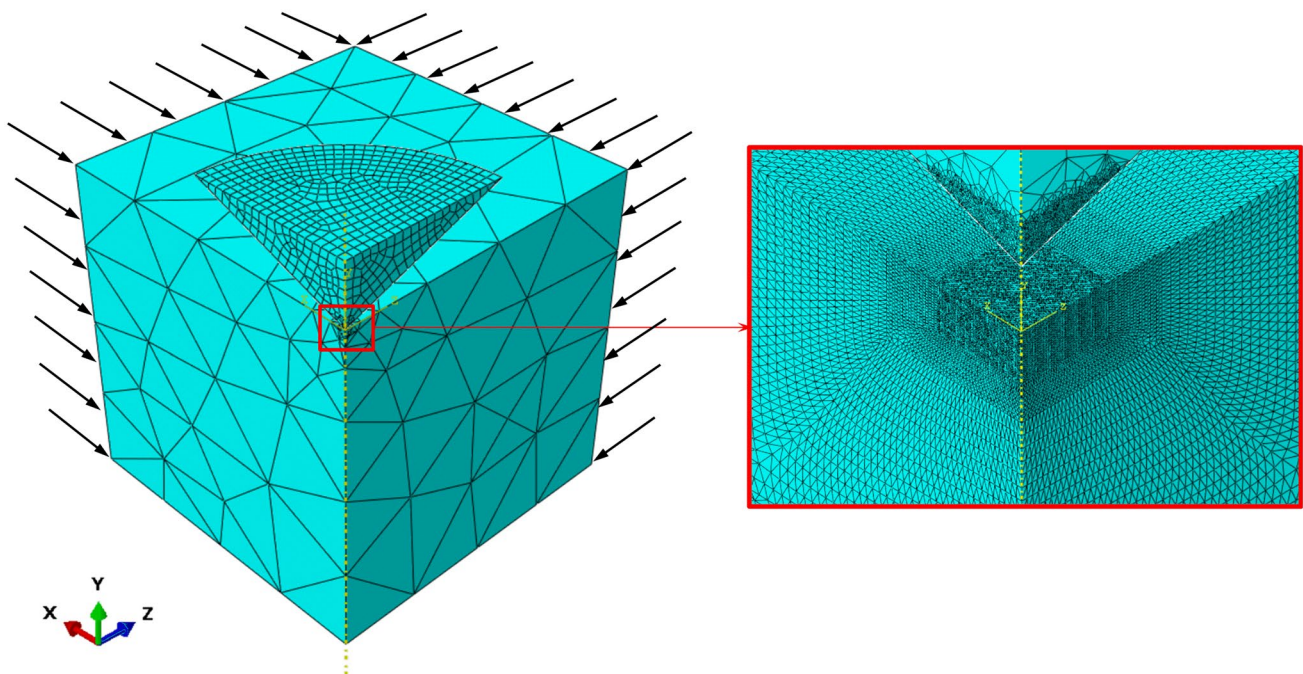


Fig. 3 FEM nanoindentation model assembly with a magnified highlight of the sample penetration zone



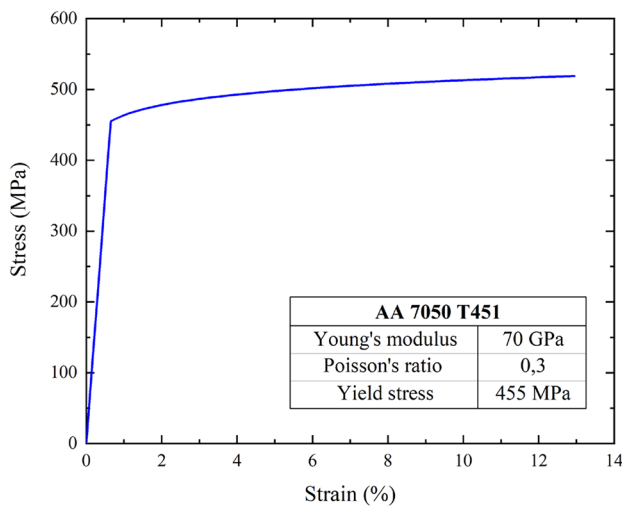


Fig. 4 Stress-strain curve of AA 7050 T451

parameters of interest, as well as the plastic flow were experimentally obtained, as reported in Fig. 4.

The maximum penetration depth for the nanoindentation experiments was set to 2000 nm, which is a typical value for metals [35]. The nanoindentation curve was obtained recording the reaction force of the indenter in the penetration direction (load) and the displacement of the sample surface penetrated by the indenter.

### Experimental Approach

Experimental investigations were carried out to validate the proposed methodology. To this aim, nanoindentations tests were done on a sample under the effect of an externally applied mechanical stress. The aim is to measure the effect of this latter on the load-penetration curve and compare the results with data obtained from the numerical finite element simulations. For the application of the mechanical stress

during the nanoindentation, a proper setup was designed and realized taking into account the following constraints:

- The dimensions of the whole device should be small enough to be fitted under the nanoindenter.
- The stress field within the area of interest must be uniform to ensure repeatable measurements.
- The device should guarantee the application of both compressive and tensile stresses for a complete analysis of the residual stresses.

The solution of this problem could be found in the four-points bending test, as depicted in Fig. 5. In fact, a uniform uniaxial compressive and tensile stress field between the supporting pins is ensured on the top and the bottom specimen surface, respectively.

However, the aim of the present work is to measure the effect of equi-biaxial residual stress field on the nanoindentation load. Consequently, a cruciform sample is proposed to generate a generically biaxial stress field, as reported in Fig. 6. This latter also reports the undeformed, Fig. 6(a), and deformed, Fig. 6(b), configuration. The geometry of the specimen is characterized by two principal bending directions. When all the loading pins move equally, the area within the four supporting pins will be subjected to uniform biaxial stress. Based on this consideration, such area would represent the investigation area.

### Experimental Setup

The geometry of the stress-generating jig was specifically designed considering the geometrical constraints of the nano-indenter platform NHT2 (Anton Paar, Austria). A 3D model of the device proposed in this work is schematically shown in Fig. 7. It is made by a chassis (bottom jig) that will be rigidly attached to the nanoindenter platform; four miniaturized load cells that are demanded to continuously

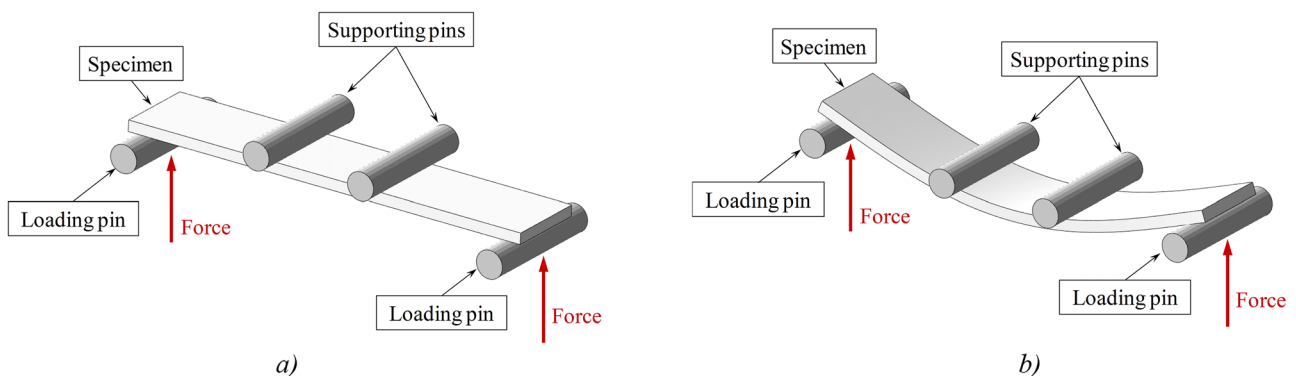
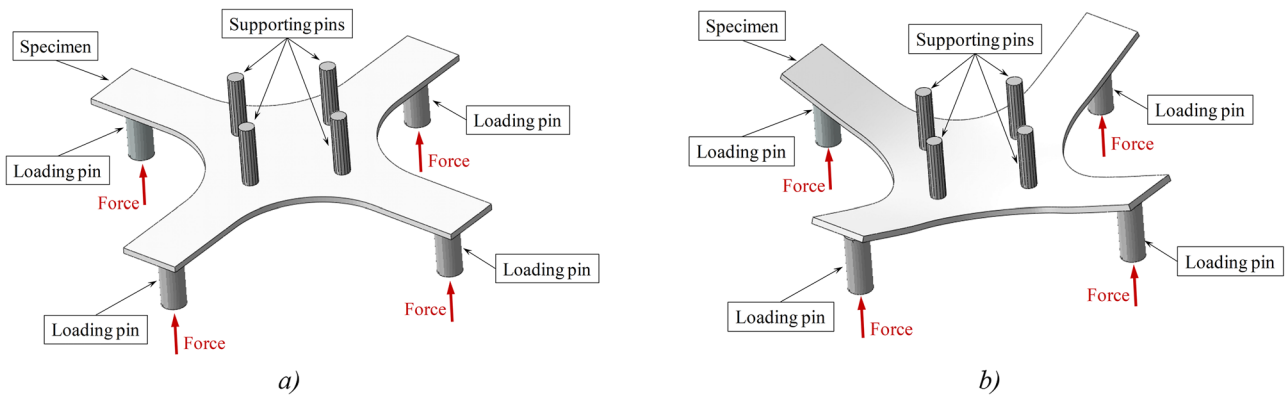


Fig. 5 Specimen for uniaxial stress. (a) undeformed configuration; (b) deformed configuration



**Fig. 6** Specimen for biaxial stress. **(a)** undeformed configuration; **(b)** deformed configuration

record the applied load, allowing to calculate the applied mechanical stress as well, but they also represent the supporting pins schematically shown in Fig. 6; bending screws that are necessary to bend the sample, as schematically shown in Fig. 6, and an upper jig that is demanded to carry the load cell and firmly stabilize the entire device. The holes, made on both the upper and bottom jigs, are required to guarantee the entrance of the indenter head for the nanoindentation tests.

According to the geometry reported in Fig. 7, the upper investigation area of the specimen is subjected to a compressive stress state whereas the bottom one is subjected to

tensile stress. Depending on the displacement of the loading pins, one can generate a generic biaxial stress field. However, if all the loading pins move equally, the induced stress field is equi-biaxial, that is the one investigated in this work.

The manufactured stress generating jig is showed in Fig. 8, together with a scheme of the data acquisition system. The specimen used in this investigation is made by AA 7050 T451, whereas the bottom and upper jigs are made by stainless steel.

The entire stress generating jig was mounted on a nanoindentation platform NHT2, Anton Paar, (load capacity 500 mN) for the experiments. In particular, nanoindentation tests were carried out using a Berkovich tip in depth control mode and

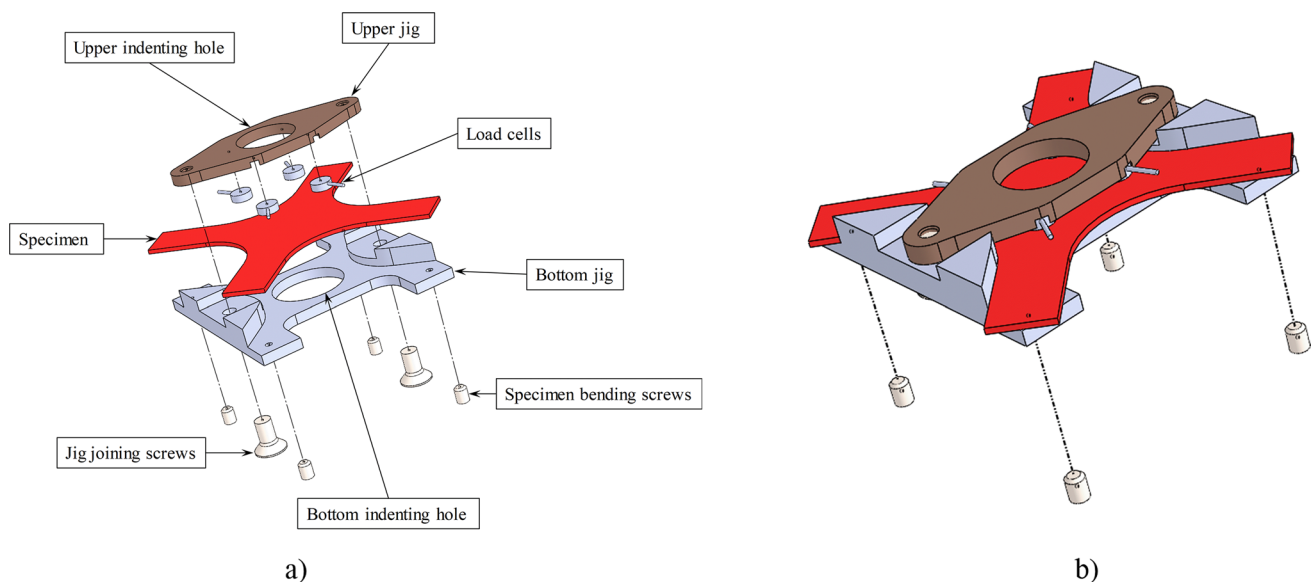


**Fig. 7** Scheme of the stress generating jig. **(a)** exploded view; **(b)** compressed view

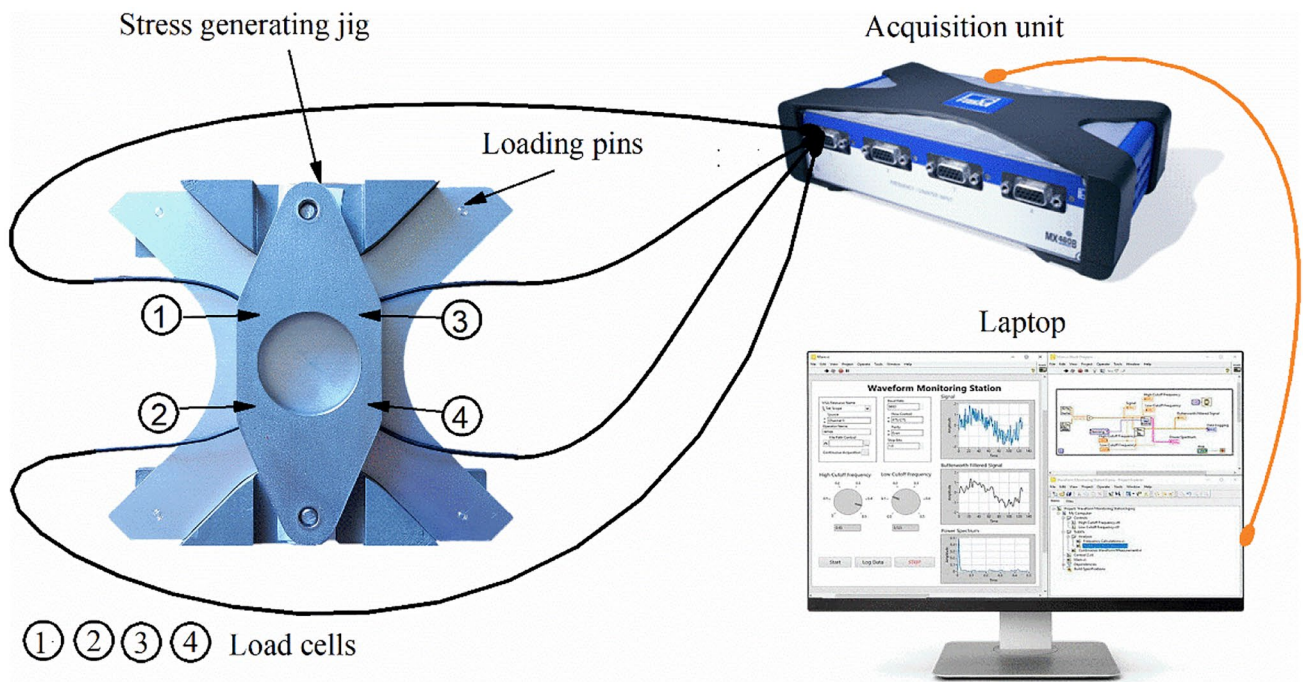


**Fig. 8** Stress generating jig and scheme of the data acquisition system

a maximum penetration depth of 2000 nm. Figure 9 shows the nanoindenter platform working on the sample installed in the stress generating jig. For each mechanical stress levels, 25 nanoindentation tests were performed for statistical purpose of the results. Figure also shows the residual imprints of the indentations. The distance between each indentation was set to 100  $\mu\text{m}$  in both the horizontal and vertical

direction to avoid measurements to interact and/or interfere each other.

**Validation Measurements**

The only load cell information cannot be used to guarantee the application of the desired mechanical stress, as

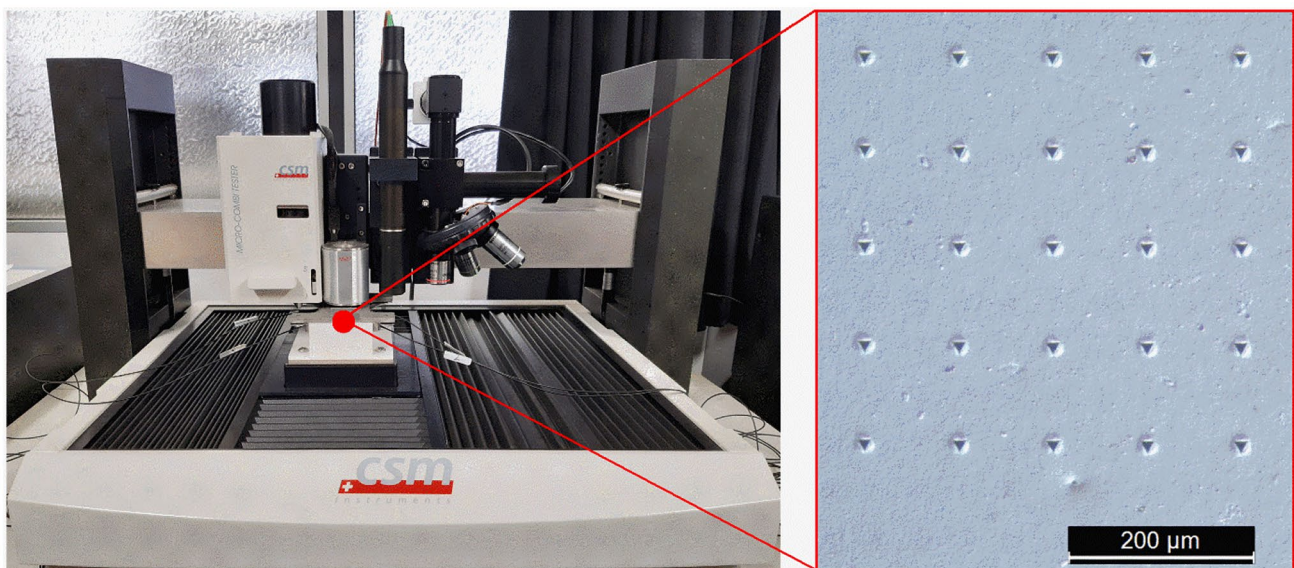


**Fig. 9** Nanoindenter NHT2 platform performing tests on the sample in the stress generating jig; figure also shows the residual imprints from nanoindentation tests, matrix of 25 Berkovich indentations



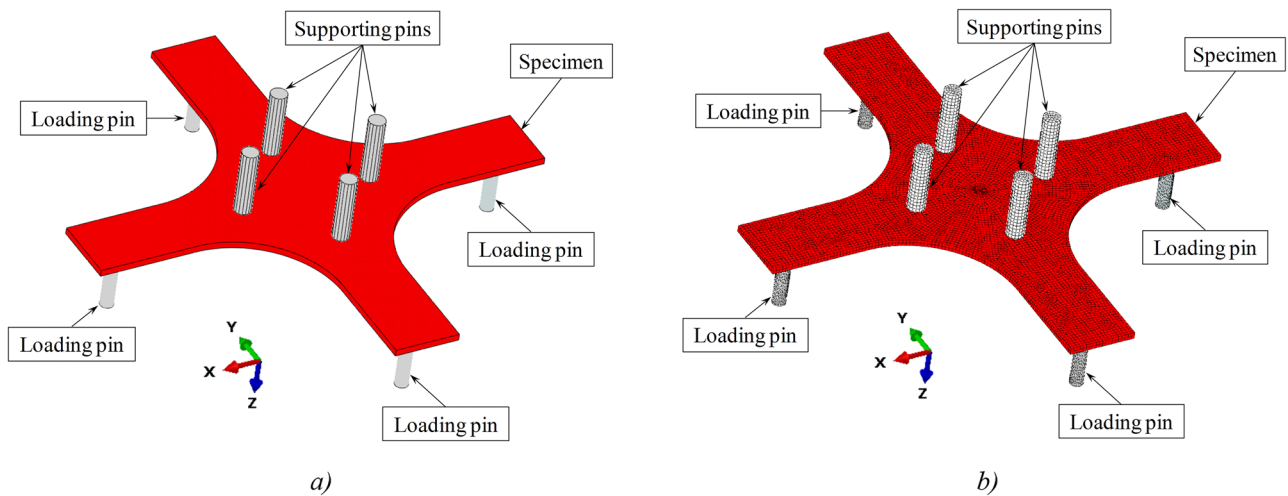


**Fig. 10** FEM model of the stress generating jig: **(a)** Assembly composed of the cruciform specimen and the loading and supporting pins; **(b)** Mesh of the whole assembly

manufacturing error and/or mechanical clearance could generate displacement misalignment within the sample. Therefore, a proper calibration/validation is required. It can be done by comparing the exact displacement field generated within the investigation area when a specific screw movement is applied with the real one obtained by the stress generating jig. A combining of numerical FEM simulations and digital image correlation (DIC) measurements would help in this direction.

For this reason, a numerical FEM model was developed to simulate the loading conditions generated by the jig, as represented in Fig. 10. It was implemented by using the commercial finite element code ABAQUS CAE

(Dassault Systemes 2020). The model is composed of the cruciform sample, four supporting pins and four loading pins. These latter were modelled as rigid cylindrical parts and represent, respectively, the specimen bending screws and the load cells. Thanks to symmetry, the simulation of a quarter model was sufficient but the whole one is represented for clearness.

The specimen was defined as a deformable part made of AA 7050 T451. Both elastic and plastic properties of the specimen material were implemented in the model, see Fig. 4.

Concerning the bodies interaction, a general contact for all parts was defined. Friction is not involved in the analysis since the parts do not slide on each other. The supporting pins

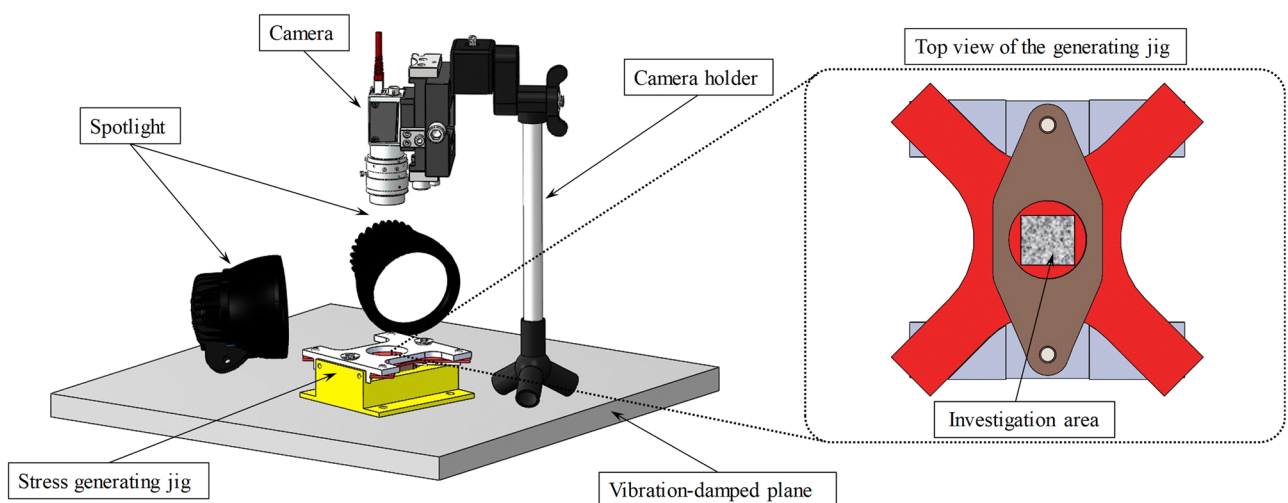


**Fig. 11** Scheme of the Digital Image Correlation (DIC) experimental setup



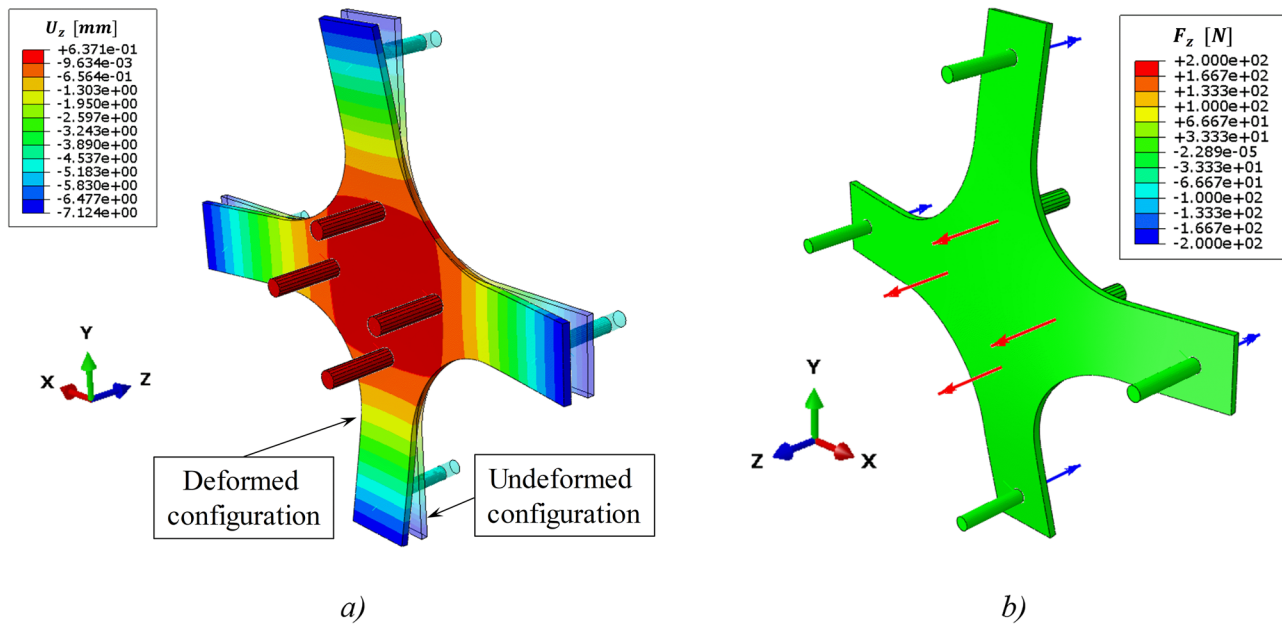


**Fig. 12** Cruciform sample FEM model results: (a) out-of-plane displacement  $U_z$  imposed along z-direction; (b) corresponding reaction force  $F_z$  at the supporting and loading pins

positions are fixed in the numerical domain whereas the loading pins can only move in the z-direction, see Fig. 10. The supporting and loading pins were discretized respectively with 355 and 726 R3D4 elements (average size 1 mm), the sample, instead, was discretized with about 15,000 C3D20 elements (average size 1 mm). Quadratic elements were used for the sample since it is subjected to flexural stress.

For the experimental measurements, the DIC technique was used. It allows to get the real displacement field of a component by comparing pictures captured on the investigation area of the sample under the effect of an external load with a stress-free reference one. Figure 11 schematically shows the employed equipment that consists of a Sony ICX 625-Prosilica GT 2450 CCD camera with a resolution of  $2448 \times 2050$  pixels along with two light sources. The focus of the images was performed using a Linos Photonics objective and a Rodagon lens f. 80 mm. Furthermore, camera spacers were adopted in order to get the magnification that allow to visualize the investigation area within the indenting holes. In these conditions a scale of approximately 90 pixels/mm was obtained. The natural pattern of the sample was used for the correlation analysis. Digital image correlation was carried out by a commercially available image correlation software (Vic-2D Correlated Solution) by setting 31 pixels for the subset size and 3 pixels for the step size. It is essential to highlight that out of plane displacements have to be expected during the experiments, therefore 3D-DIC

should be used estimate the data correctly. However, considering that the only aim was to qualitatively verify the capability of the setup to apply equi-biaxial stresses within the sample, 2D-DIC measurements were done. In this case, the in-plane displacements will represent a projection of the total displacements on the focus plane of the camera, but for the sake of this work it was sufficient.

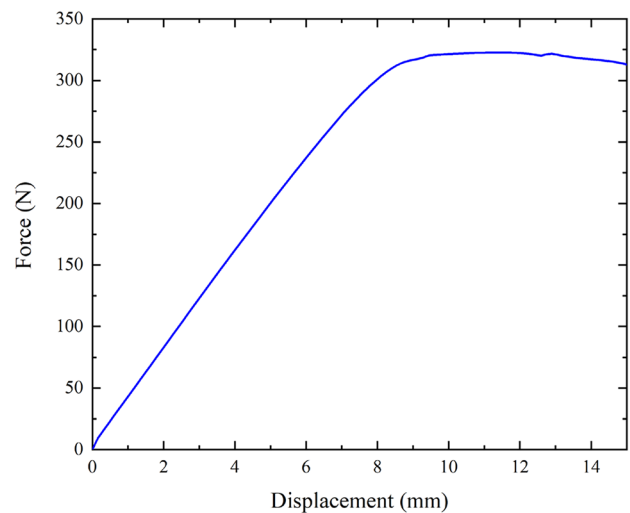


**Fig. 13** Reaction force at the supporting pins as a function of the displacement of the loading pins

## Results and Discussion

The results obtained from the FEM model of the cruciform sample, together with the experimentally DIC measured displacement fields, are reported in Figs. 12, 15, 16 and 17. In particular, Fig. 12(a) shows the out-of-plane displacement  $U_z$  of the sample (z-direction in the figure) when the loading

pins move 5 mm along the z-direction; Fig. 12(b), instead, shows the corresponding reaction forces  $F_z$  measured at the loading and supporting pins.

The reaction force  $F_z$ , measured at the supporting pins, as a function of the applied displacement of the loading pins  $U_z$  is reported in Fig. 13. Its trend is almost linear up to 320 N, that correspond to 8 mm of displacement, then it tends to slowly

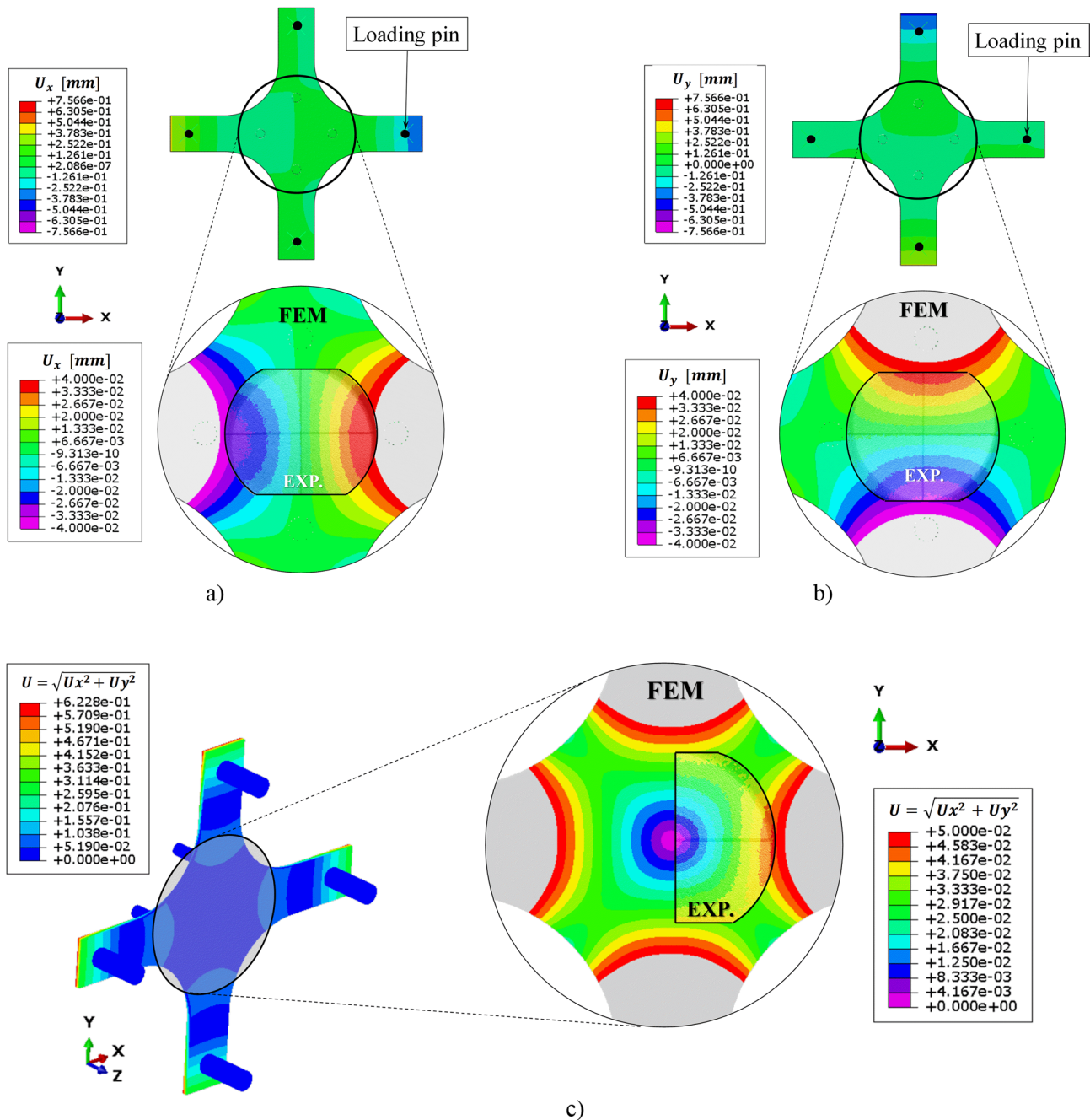


**Fig. 14** In-plane displacement field generated on the tensile side of the sample: (a) horizontal  $U_x$  (mm) displacements along the x-direction; (b) vertical  $U_y$  (mm) displacements along the y-direction; (c)  $U$  (mm) magnitude of the in-plane displacement ( $U = \sqrt{U_x^2 + U_y^2}$ ). These results are referred to a movement of 5 mm of the loading pins (load recorded by load cells 200 N). A comparison between FEM and DIC experimental results is presented

decrease as yielding mechanisms occurred within the sample. Based on this information, loading pins displacement has always been kept below the critical value of 8 mm.

Figures 14 show both the numerical and experimental in-plane displacements of the tensile side of the sample when the loading pins are moved for 5 mm, corresponding to a reaction force of 200 N. In particular, Fig. 14(a), (b) show the horizontal  $U_x$  and vertical  $U_y$  displacement, respectively,

along x- and y- direction. Figure 14(c) shows the magnitude of both the numerical and experimental in-plane displacement  $U$ , calculated as:

$$U = \sqrt{U_x^2 + U_y^2} \tag{2}$$

Figures 15 show both the numerical and experimental in-plane displacements of the compression side of the sample

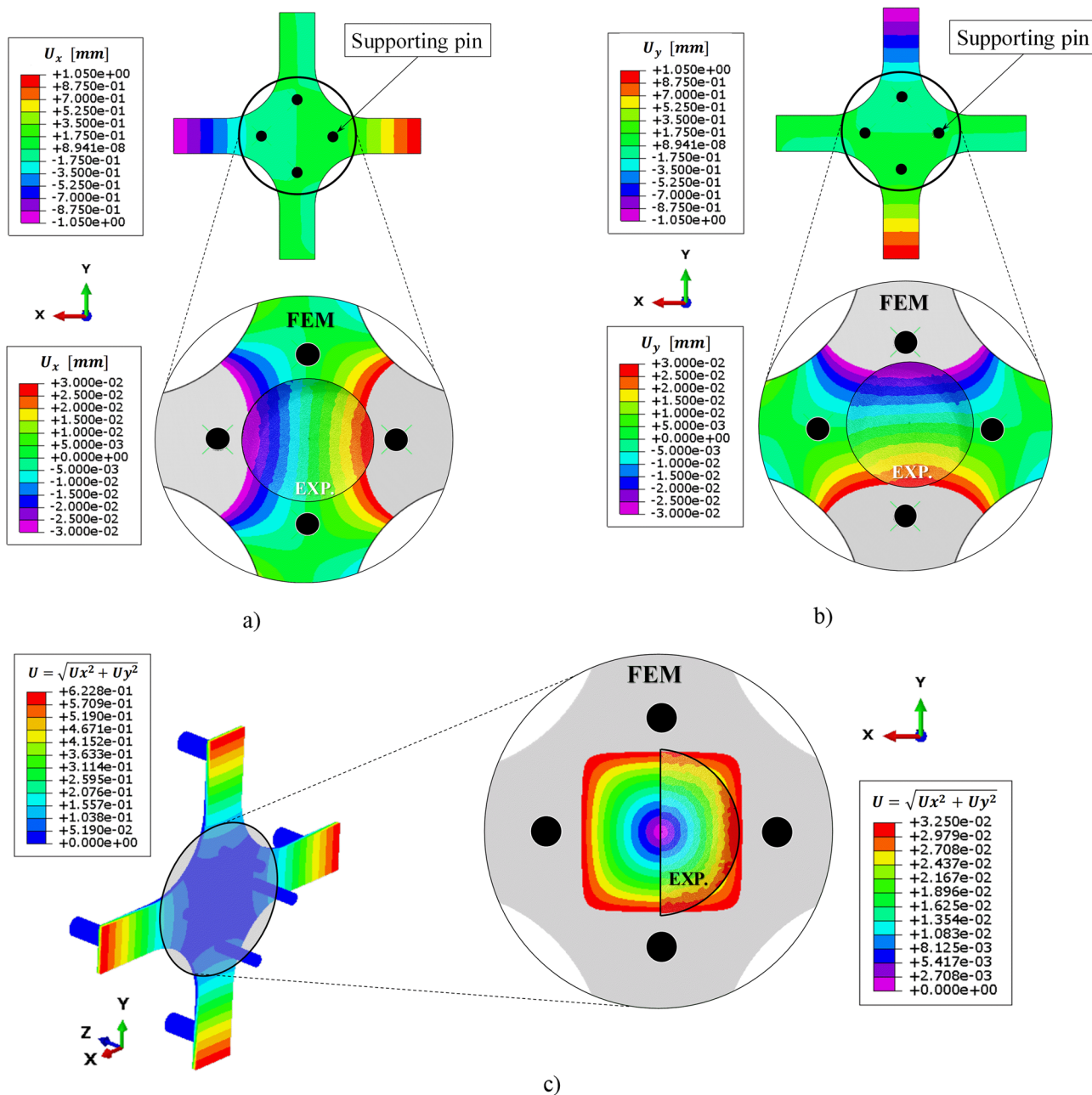


**Fig. 15** In-plane displacement field generated on the compression side of the sample: (a) horizontal  $U_x$  (mm) displacement along the x-direction; (b) vertical  $U_y$  (mm) displacement along the y-direction; (c)  $U$  (mm) magnitude of the in-plane displacement ( $U = \sqrt{U_x^2 + U_y^2}$ ). These results are referred to a movement of 5 mm of the loading pins (load recorded by load cells 200 N). A comparison between FEM and DIC experimental results is presented

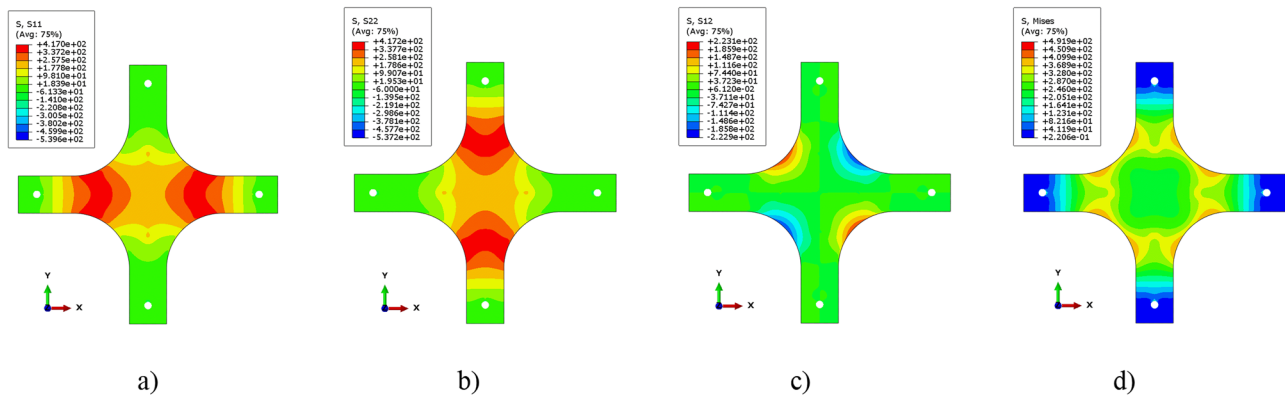


**Fig. 16** In-plane stress field on the tensile surface of the sample: (a) S11(MPa) along x-directions; (b) S22(MPa) along y-direction; (c) S12 (MPa) shear component in x-y plane; (d) Mises equivalent stress (MPa). These results are referred to a movement of 5 mm of the loading pins (load recorded by load cells 200 N)

when the loading pins are moved for 5 mm, corresponding to a reaction force of 200 N. In particular, Fig. 15(a), (b) show the horizontal  $U_x$  and vertical  $U_y$  displacement, respectively, along x- and y- direction. Figure 15(c) reports the magnitude of the in-plane displacement  $U$ , calculated using equation (2).

Figures 14 and 15 clearly show that the DIC experimental measurements well match the numerical predictions. Therefore, it is possible to assert that the designed stress generating jig is able to generate the desired stress field within the sample and it can be used for the calibration/validation of the proposed model.

Figures 16 and 17 show the stress field induced within the sample, on the tensile and compression surface of the sample, respectively, obtained by numerical analyses. Focusing on the region of interest, one can observe that both the principal stress components S11 and S22, measured along x- and y-direction, respectively, have the same value in both the tensile side (240 MPa, see Fig. 16(a), (b)) and the compressive one

(-205 MPa, see Fig. 17(a), (b)), no shear stress S12 in the x-y plane, Figs. 16(c) and 17(c), are observed and the equivalent Von Mises stress, Figs. 16(d) and 17(d), is uniform.

Figures also revealed that within the investigation region the tensile stress values are greater than the compressive ones due to the particular geometry of the sample. Moreover, Figs. 16 and 17 show that yielding will occur out of the indenting zone.

Figure 18 shows the S11 stress evolution as a function of the displacement applied on the loading pins, obtained at the middle point of the cruciform sample. Both the tensile and compression side are reported. Figure shows that stress is linear before yielding occurs and the tensile stress is greater than the compressive one.

Once the relation between the loading pins displacement and stress is known and after verifying that the induced stress field is equi-biaxial and uniform, nanoindentations were carried out. Figure 19 shows the comparison between

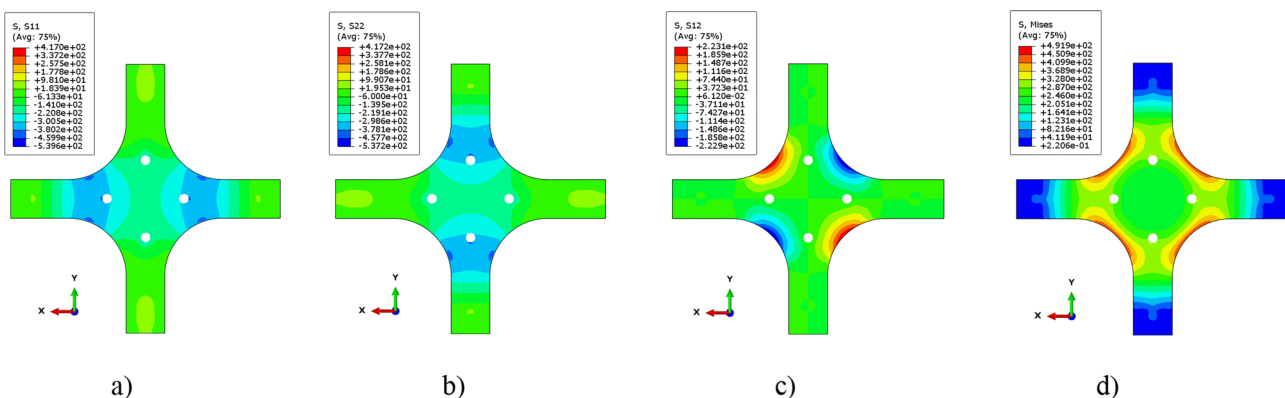


**Fig. 17** In-plane stress field on the compression surface of the sample: (a) S11(MPa) along x-directions; (b) S22(MPa) along y-direction; (c) S12 (MPa) shear component in x-y plane; (d) Mises equivalent stress (MPa). These results are referred to a movement of 5 mm of the loading pins (load recorded by load cells 200 N)



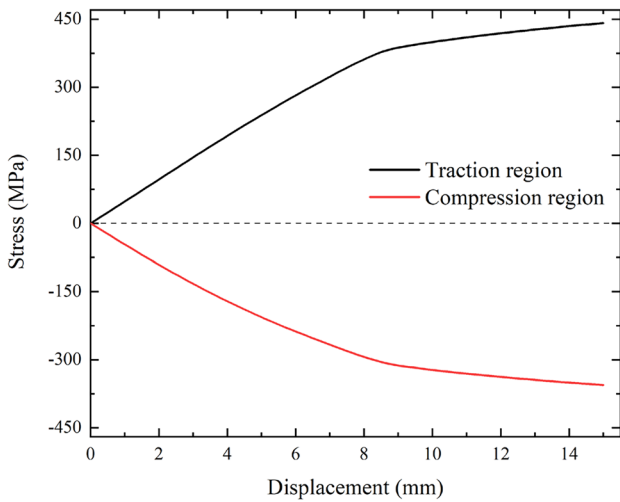


**Fig. 18** In-plane stress components in the traction and compression regions as a function of the displacement of the loading pins. Due to the symmetry conditions, the stress components in-plane are equal

the experimental and the numerical nanoindentation curves obtained on the stress-free sample when a maximum penetration depth of 2000 nm is applied. Results revealed that the numerical model accurately simulates the nanoindentation process.

Figure 20 shows the numerical nanoindentation response of the same sample under the effect of different equi-biaxial stresses. The aim is to investigate the influence of the stress level on the loading path of the nanoindentation curves and, particularly, on the peak load. Within the figure, the dotted line represents the load-penetration response of the stress-free sample, the green lines the ones of the sample under tensile

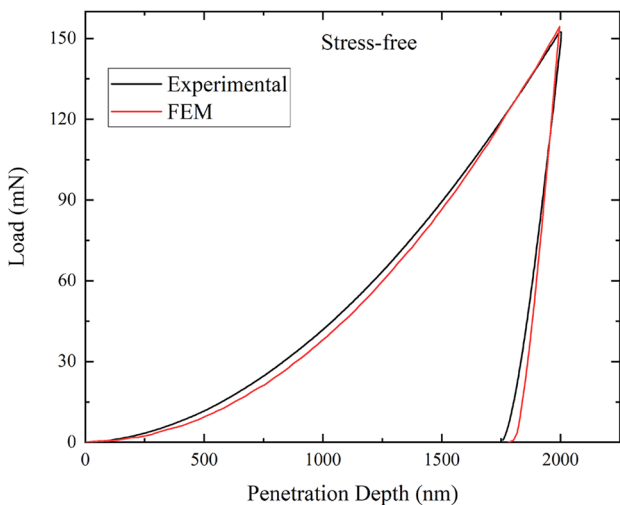


**Fig. 19** Nanoindentation curve of the stress-free sample. Both the experimental and the FEM numerical curves are represented

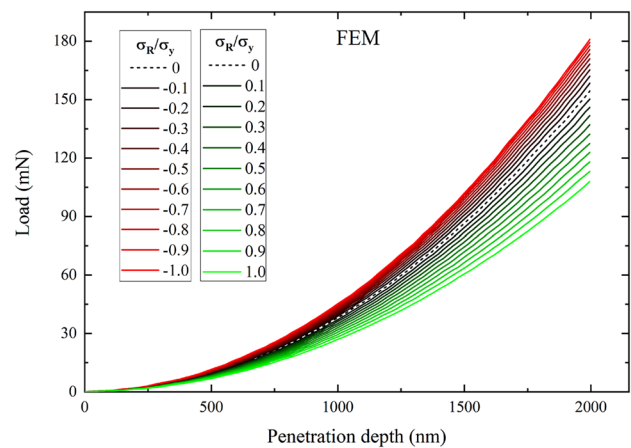
stress fields and the red lines the response of the sample under compressive stress fields. The ratio between residual stress  $\sigma_R$  and yield stress  $\sigma_y$  ranges from -1.0 to 1.0 with 0.1 steps.

Figure 20 confirms that tensile stress has a greater effect on the nanoindentation peak load compared to compressive stress, as also reported in literature [8, 30]. For compressive stress field, the effect of residual stress on the nanoindentation peak load tends to decrease when the magnitude of the stress increases. This is due to the stress field that the nanoindentation process induces itself. During the sample penetration, in fact, a compressive stress state is produced beneath the indenter. The nanoindentation stress field interacts with the residual stress field and, consequently, the effect of tensile residual stress field (opposite in sign with the nanoindentation stress field) is greater than the compressive residual stress field.

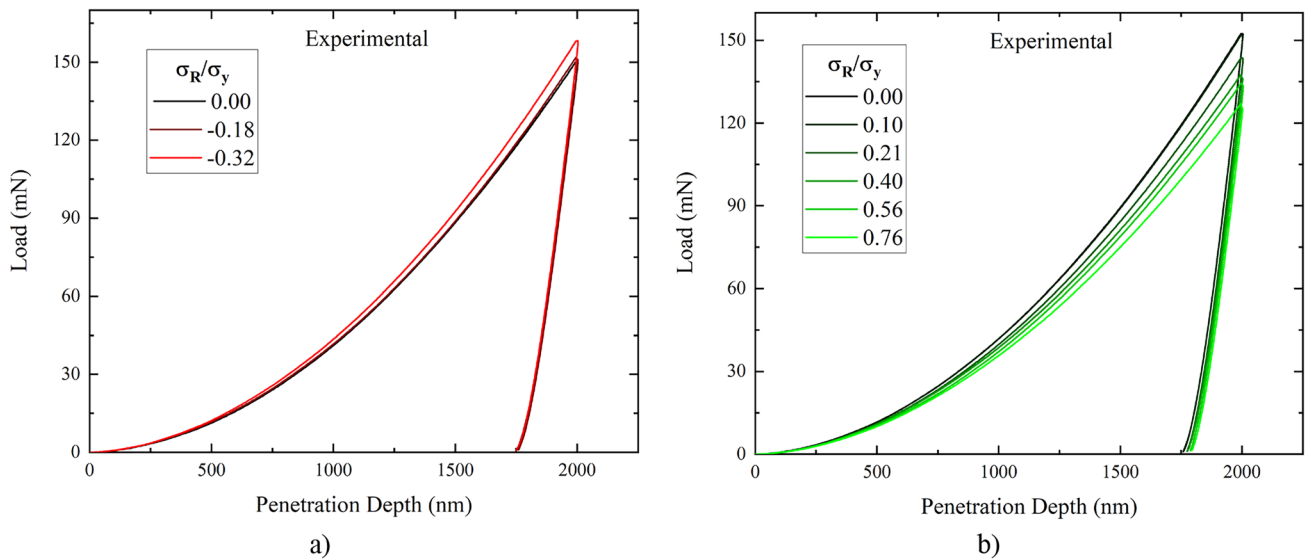
Figure 21 shows the experimental nanoindentation curves obtained using the stress generating jig for different stress level. In particular, Fig. 21(a) is referred to compressive stress fields, whereas Fig. 21(b) is referred to tensile stress fields. Results revealed a trend very similar to the response obtained by the numerical simulations confirming that the stress generating jig is able to well apply the desired stress field within the region of interest.

Figure 22 shows the peak load variation with the residual stress. Both FEM numerical and experimental results are presented. For the stress-free sample, corresponding to  $\sigma_R/\sigma_y = 0$ , measurements were carried out on both the upper and lower surface of the sample. As expected, these measurements are almost identical.

Results revealed a good match between the numerical data and the experimental prediction. A very slight difference was obtained for tensile stress field, whereas for the



**Fig. 20** Nanoindentation curves numerically obtained for different stress level. The residual stress  $\sigma_R$  ratio yield stress  $\sigma_y$  ranges from -1.0 to 1.0. Only the loading portion of the nanoindentation curves is represented for clearness



**Fig. 21** Nanoindentation curves experimentally derived for various stress level; **(a)** compression stress; **(b)** tensile stress

compression stress field, the FEM-experimental difference is a bit more pronounced. The effect of the compressive stress state, in fact, is more difficult to be observed experimentally for the following reasons:

- The magnitude of the nanoindentation peak load variation is reduced for compressive stress field compared to the tensile one. Consequently, the model is less sensitive to compression stress.
- During the nanoindentation tests, a reference header ring touches the specimen applying a bit pressure over the involved zone. This can produce a relaxation of the

compressive stress state as the ring pressure tends to re-align the sample in the contact zone.

- High compressive stress level cannot be tested using nanoindenter because of the curvature of the sample. In fact, the extremities of the cruciform specimen obviously raise because of the displacement of the loading pins. When this displacement exceeds a threshold, measurements are not possible. The threshold is determined by the specific design features of the nanoindenter platform NHT2. Furthermore, when the bending specimen screws move, the induced tensile stress magnitude is greater than the compressive one.

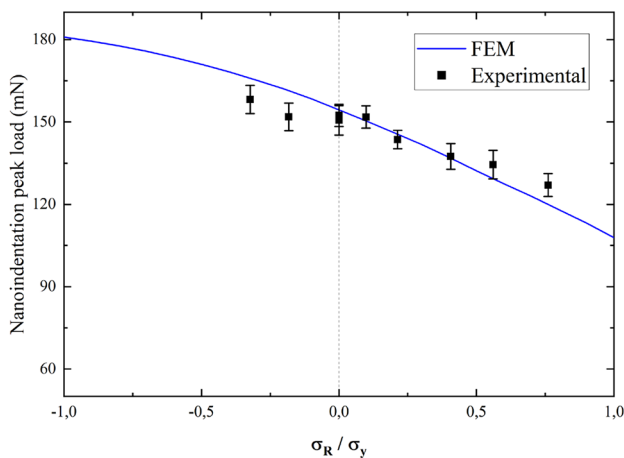


**Fig. 22** Relation between nanoindentation peak load and stress level. The maximum penetration depth of the nanoindentation tests was set to 2000 nm

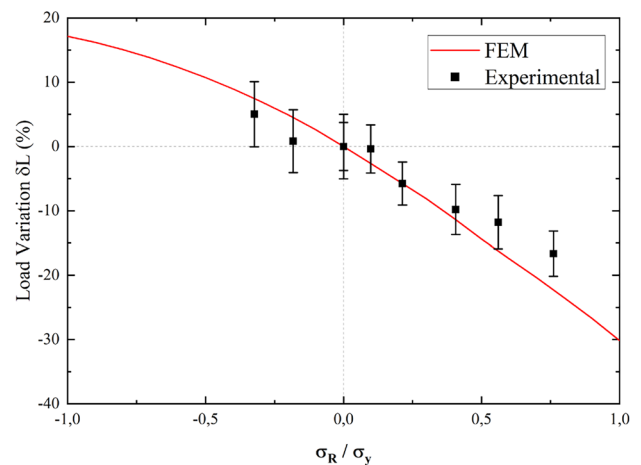


**Fig. 23** Relation between nanoindentation load variation  $\delta L$  and stress level

For all these reasons, a slightly bigger error was expected for compressive stress field than for tensile one. In any case, the magnitude of the committed error is widely acceptable.

It is important to point out that the peak load depends on the applied maximum penetration depth. It could be most useful apply equation (1) and identify the relation between RS and the relative nanoindentation load variation  $\delta L$  that is independent of the maximum penetration depth. This relation is reported in Fig. 23. Since  $\delta L$  is an indirect measurement, its standard variation is significant, and this could lead to measurements error. Despite this concern, the experimental measures well fit the FEM results. Similar to the evidence of Fig. 22, even in this case, the effect of tensile stress is obviously greater than the compressive stress effect.

## Conclusions

In this paper, a method for the measurement of equi-biaxial residual stress fields via instrumented nanoindentation is presented. The method was experimentally validated for an AA 7050 T451 sample.

The main idea was to use the nanoindentation peak load as residual stress estimator. In detail, it can be assumed that the variation of the nanoindentation peak load from a sample under the effect of residual stresses compared to a reference one is proportional to RS. If this relation is known, the RS can be estimated by a simple non-destructive nanoindentation test. The relation between the peak load variation and RS was found by finite element simulations and the obtained results were experimentally validated. To this aim an ad-hoc stress generating jig was designed and manufactured. It allowed to induce a desired equi-biaxial stress field over a specimen and simultaneously execute nanoindentation tests to measure the peak load variation. Experimental measurements demonstrated good match with numerical simulations confirming the accuracy of the proposed methodology. It is important to point out that the methodology is also applicable to non equi-biaxial residual stresses, even though in such cases a mean value of the in-plane stress is provided. The generalization to non-equi-biaxial residual stress fields requires further developments of the model and additional data. These latter can be obtained by using a non-axisymmetric indenter tip and additional information in different planes. All these aspects will be explored in a future work.

The strategy for the RS measurement here presented is simply applicable, also on industrial parts, and it just require an initial calibration for the material under investigation. In particular, if the properties of the material under investigation are known, a finite element analysis of the real component can be carried out, with the only condition that the overall geometrical size of the part must be two orders of magnitude

greater than the selected indentation depth, to avoid edge effects and to allow the correct evolution of the process zone. The cruciform sample could be required only for validating the numerical results when a new material is investigated.

Future developments of the present work will involve the application of the proposed methodology and the comparison with results obtained by most conventional RS measurement technique.

**Acknowledgements** Nanoindentation experiments, tensile tests and full-field measurements were carried out in the ‘‘MaTeRiA Laboratory’’ (University of Calabria), funded with ‘‘Pon Ricerca e Competitivit  2007/2013’’.

**Author Contributions** Alessia Greco: Conceptualization, Methodology, Software, Experiments, Validation, Formal analysis, Writing – original draft, Visualization. Emanuele Sgambitterra: Conceptualization, Methodology, Validation, Formal analysis, Writing –review & editing, Visualization. Franco Furgiuele: Conceptualization, Methodology, Resources, Writing – review & editing, Supervision. Domenico Furfari: Conceptualization, Methodology, Resources, Writing –review & editing, Supervision.

**Funding** Open access funding provided by Universit  della Calabria within the CRUI-CARE Agreement.

**Data Availability** The raw data required to reproduce these findings are available from authors on request.

## Declarations

**Ethical Approval** Not applicable.

**Conflict of Interest** The authors declare that they have no known competing financial interests or personal relationships that could have appeared to influence the work reported in this paper.

**Open Access** This article is licensed under a Creative Commons Attribution 4.0 International License, which permits use, sharing, adaptation, distribution and reproduction in any medium or format, as long as you give appropriate credit to the original author(s) and the source, provide a link to the Creative Commons licence, and indicate if changes were made. The images or other third party material in this article are included in the article’s Creative Commons licence, unless indicated otherwise in a credit line to the material. If material is not included in the article’s Creative Commons licence and your intended use is not permitted by statutory regulation or exceeds the permitted use, you will need to obtain permission directly from the copyright holder. To view a copy of this licence, visit <http://creativecommons.org/licenses/by/4.0/>.

## References

1. Withers PJ, Bhadeshia HKDH (2001) Residual stress. Part 1 – Measurement techniques. *Mater Sci Technol* 17:355–65. <https://doi.org/10.1179/026708301101509980>
2. Withers PJ, Bhadeshia HKDH (2001) Residual stress. Part 2 – Nature and origins. *Mater Sci Technol* 17:366–75. <https://doi.org/10.1179/026708301101510087>
3. Tabatabaeian A, Ghasemi AR, Shokrieh MM, Marzbanrad B, Baraheni M, Fotouhi M (2022) Residual Stress in Engineering Materials: A Review. *Adv Eng Mater* 24:2100786. <https://doi.org/10.1002/adem.202100786>

4. Kuang W, Miao Q, Ding W, Li H (2022) A short review on the influence of mechanical machining on tribological and wear behavior of components. *Int J Adv Manuf Technol* 120:1401–1413. <https://doi.org/10.1007/s00170-022-08895-w>
5. Qutaba S, Asmelash M, Saptaji K, Azhari A (2022) A review on peening processes and its effect on surfaces. *Int J Adv Manuf Technol* 120:4233–4270. <https://doi.org/10.1007/s00170-022-09021-6>
6. Guo J, Fu H, Pan B, Kang R (2021) Recent progress of residual stress measurement methods: A review. *Chin J Aeronaut* 34:54–78. <https://doi.org/10.1016/j.cja.2019.10.010>
7. Huang X, Liu Z, Xie H (2013) Recent progress in residual stress measurement techniques. *Acta Mech Solida Sin* 26:570–583. [https://doi.org/10.1016/S0894-9166\(14\)60002-1](https://doi.org/10.1016/S0894-9166(14)60002-1)
8. Greco A, Sgambitterra E, Furgiuele F (2021) A new methodology for measuring residual stress using a modified Berkovich nano-indenter. *Int J Mech Sci* 207:106662. <https://doi.org/10.1016/j.ijmecsci.2021.106662>
9. Zhu L-N, Xu B-S, Wang H-D, Wang C-B (2015) Measurement of Residual Stresses Using Nanoindentation Method. *Crit Rev Solid State Mater Sci* 40:77–89. <https://doi.org/10.1080/10408436.2014.940442>
10. Jang J (2009) Estimation of residual stress by instrumented indentation: A review. *J Ceram Process Res* 10:391–400
11. Suresh S, Giannakopoulos AE (1998) A new method for estimating residual stresses by instrumented sharp indentation. *Acta Mater* 46:5755–5767. [https://doi.org/10.1016/S1359-6454\(98\)00226-2](https://doi.org/10.1016/S1359-6454(98)00226-2)
12. Lee Y-H, Kwon D (2004) Estimation of biaxial surface stress by instrumented indentation with sharp indenters. *Acta Mater* 52:1555–1563. <https://doi.org/10.1016/j.actamat.2003.12.006>
13. Swadener JG, Taljat B, Pharr GM (2001) Measurement of residual stress by load and depth sensing indentation with spherical indenters. *J Mater Res* 16:2091–2102. <https://doi.org/10.1557/JMR.2001.0286>
14. Xu Z-H, Li X (2005) Influence of equi-biaxial residual stress on unloading behaviour of nanoindentation. *Acta Mater* 53:1913–1919. <https://doi.org/10.1016/j.actamat.2005.01.002>
15. Xu Z-H, Li X (2006) Estimation of residual stresses from elastic recovery of nanoindentation. *Phil Mag* 86:2835–2846. <https://doi.org/10.1080/14786430600627277>
16. Lu Z, Feng Y, Peng G, Yang R, Huan Y, Zhang T (2014) Estimation of surface equi-biaxial residual stress by using instrumented sharp indentation. *Mater Sci Eng A* 614:264–272. <https://doi.org/10.1016/j.msea.2014.07.041>
17. Wang Q, Ozaki K, Ishikawa H, Nakano S, Ogiso H (2006) Indentation method to measure the residual stress induced by ion implantation. *Nucl Instrum Methods Phys Res B* 242:88–92. <https://doi.org/10.1016/j.nimb.2005.08.008>
18. Pham T-H, Kim S-E (2017) Determination of equi-biaxial residual stress and plastic properties in structural steel using instrumented indentation. *Mater Sci Eng, A* 688:352–363. <https://doi.org/10.1016/j.msea.2017.01.109>
19. Moharrami R, Sanayei M (2020) Improvement of indentation technique for measuring general biaxial residual stresses in austenitic steels. *Precis Eng* 64:220–227. <https://doi.org/10.1016/j.precisioneng.2020.04.011>
20. Xiao L, Ye D, Chen C (2014) A further study on representative models for calculating the residual stress based on the instrumented indentation technique. *Comput Mater Sci* 82:476–482. <https://doi.org/10.1016/j.commatsci.2013.10.014>
21. Moharrami R, Sanayei M (2020) Developing a method in measuring residual stress on steel alloys by instrumented indentation technique. *Measurement* 158:107718. <https://doi.org/10.1016/j.measurement.2020.107718>
22. Hosseinzadeh AR, Mahmoudi AH (2019) An approach for Knoop and Vickers indentations to measure equi-biaxial residual stresses and material properties: A comprehensive comparison. *Mech Mater* 134:153–164. <https://doi.org/10.1016/j.mechmat.2019.04.010>
23. Wang Q, Ji B, Fu Z, Xu Z (2021) Experimental study on the determination of welding residual stress in rib-deck weld by sharp indentation testing. *Thin-Walled Struct* 161:107516. <https://doi.org/10.1016/j.tws.2021.107516>
24. Moharrami R, Sanayei M (2020) Numerical study of the effect of yield strain and stress ratio on the measurement accuracy of biaxial residual stress in steels using indentation. *J Market Res* 9:3950–3957. <https://doi.org/10.1016/j.jmrt.2020.02.021>
25. Peng W, Jiang W, Sun G, Yang B, Shao X, Tu S-T (2022) Biaxial residual stress measurement by indentation energy difference method: Theoretical and experimental study. *Int J Press Vessel Pip* 195:104573. <https://doi.org/10.1016/j.ijpvp.2021.104573>
26. Lee J, Lee K, Lee S, Kwon OM, Kang W-K, Lim J-I et al (2021) Application of Macro-Instrumented Indentation Test for Superficial Residual Stress and Mechanical Properties Measurement for HY Steel Welded T-Joints. *Materials* 14:2061. <https://doi.org/10.3390/ma14082061>
27. Xue H, Jia Y-L, Lu J-Z, Wang S, Wang Z, Wang S (2022) An approach for obtaining surface residual stress based on indentation test and strain measurement. *Mater Test* 64:220–227. <https://doi.org/10.1515/mt-2021-2037>
28. Khan MK, Fitzpatrick ME, Hainsworth SV, Edwards L (2011) Effect of residual stress on the nanoindentation response of aerospace aluminium alloys. *Comput Mater Sci* 50:2967–2976. <https://doi.org/10.1016/j.commatsci.2011.05.015>
29. Lepienski CM, Pharr GM, Park YJ, Watkins TR, Misra A, Zhang X (2004) Factors limiting the measurement of residual stresses in thin films by nanoindentation. *Thin Solid Films* 447–448:251–257. [https://doi.org/10.1016/S0040-6090\(03\)01103-9](https://doi.org/10.1016/S0040-6090(03)01103-9)
30. Sakharova NA, Prates PA, Oliveira MC, Fernandes JV, Antunes JM (2012) A Simple Method for Estimation of Residual Stresses by Depth-Sensing Indentation. *Strain* 48:75–87. <https://doi.org/10.1111/j.1475-1305.2010.00800.x>
31. Rickhey F, Lee JH, Lee H (2015) A contact size-independent approach to the estimation of biaxial residual stresses by Knoop indentation. *Mater Des* 84:300–312. <https://doi.org/10.1016/j.matdes.2015.06.119>
32. Rahimian Kooloor S, Karimzadeh A, Tamin M, Abd SM (2018) Effects of Sample and Indenter Configurations of Nanoindentation Experiment on the Mechanical Behavior and Properties of Ductile Materials. *Metals (Basel)* 8:421. <https://doi.org/10.3390/met8060421>
33. Celentano DJ, Guelorget B, François M, Cruchaga MA, Slimane A (2012) Numerical simulation and experimental validation of the microindentation test applied to bulk elastoplastic materials. *Model Simul Mat Sci Eng* 20:045007. <https://doi.org/10.1088/0965-0393/20/4/045007>
34. Fischer-Cripps AC (2011) *Nanoindentation*. Springer
35. Nguyen N-V, Pham T-H, Kim S-E (2018) Characterization of strain rate effects on the plastic properties of structural steel using nanoindentation. *Constr Build Mater* 163:305–314. <https://doi.org/10.1016/j.conbuildmat.2017.12.122>

**Publisher's Note** Springer Nature remains neutral with regard to jurisdictional claims in published maps and institutional affiliations.